Temperature-mediated transition from Dyakonov surface waves to surface-plasmon-polariton waves

IEEE Photonics Journal
An IEEE Photonics Society Publication

Open Access

Temperature–Mediated Transition From Dyakonov Surface Waves to Surface–Plasmon–Polariton Waves

Volume 8, Number 5, October 2016

Tom G. Mackay
Akhlesh Lakhtakia

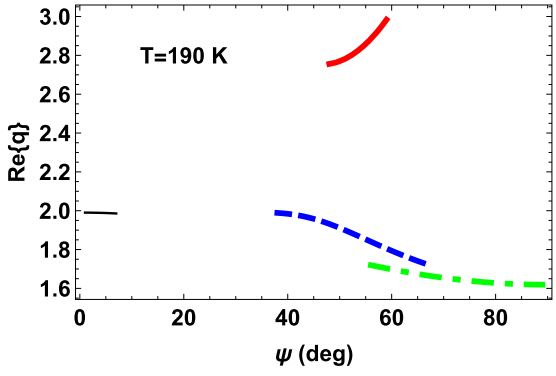

DOI: 10.1109/JPHOT.2016.2611700
1943-0655

IEEE photonics SOCIETY

IEEE

Temperature–Mediated Transition From Dyakonov Surface Waves to Surface–Plasmon–Polariton Waves

Tom G. Mackay[1,2] **and Akhlesh Lakhtakia**[2]

[1]School of Mathematics and Maxwell Institute for Mathematical Sciences, University of Edinburgh, Edinburgh EH9 3FD, UK
[2]NanoMM—Nanoengineered Metamaterials Group, Department of Engineering Science and Mechanics, Pennsylvania State University, University Park, PA 16802–6812 USA

DOI:10.1109/JPHOT.2016.2611700

Manuscript received August 11, 2016; revised September 15, 2016; accepted September 17, 2016. Date of current version October 10, 2016. The work of T. G. Mackay was supported by the EPSRC under Grant EP/M018075/1. The work of A. Lakhtakia was supported in part by the Charles Godfrey Binder Endowment at the Pennsylvania State University, and in part by the United States National Science Foundation under Grant DMS-1619901. Corresponding author: Tom G. Mackay (T.Mackay@ed.ac.uk).

Abstract: The propagation of electromagnetic surface waves, guided by the planar interface of a temperature-sensitive isotropic material and a temperature-insensitive uniaxial material, each characterized by a relative permittivity dyadic, was investigated theoretically for the case of the optic axis of the uniaxial partnering material lying wholly in the interface plane. On raising the temperature, the isotropic partnering material (namely, InSb) transforms from a weakly dissipative dielectric material to a metal in the terahertz frequency regime. Correspondingly, the surface waves change from being Dyakonov surface waves to being surface–plasmon–polariton (SPP) waves. Numerical studies revealed that modest changes in temperature could result in dramatic changes in the numbers of propagating surface waves, their angular existence domains, their propagation constants, and their decay constants. Whereas multiple Dyakonov surface waves may propagate in a specific direction if at least one of the two partnering materials is dissipative, at most one SPP wave can propagate in a specific direction.

Index Terms: Dissipative materials, Dyakonov surface waves, surface–plasmon–polariton waves, temperature control.

1. Introduction

Various types of electromagnetic surface wave may be guided by the planar interface of two dissimilar materials [1]. For example, if one of the two partnering materials is a metal and the other is a dielectric material, then surface–plasmon–polariton (SPP) waves may be guided by the interface [2], [3]. Alternatively, if one of the two partnering materials is an isotropic dielectric material and the other is an anisotropic dielectric material, then Dyakonov surface waves may be guided by the interface [4]–[7]. Typically, SPP waves can propagate in a wide range of directions (even all directions) in the interface plane [1], whereas Dyakonov surface waves propagate in a small range of directions in the interface plane [8]. Such surface waves may be exploited for applications in optical sensing [9]–[11], communication [12], [13], and harvesting solar energy [14], [15], among other applications.

The scenario wherein both partnering materials are dissipative has received little attention from researchers. However, as demonstrated in the following sections, in this scenario a richer palette of surface-wave characteristics is supported as compared to the scenario where one or both of the partnering materials is nondissipative. The particular issue under investigation herein is the transition from Dyakonov surface waves to SPP waves that can be induced by varying the temperature. To this end, the planar interface of a temperature-sensitive isotropic material and a temperature-insensitive uniaxial material is considered, each material characterized by a relative permittivity dyadic [16] and the optic axis of the uniaxial partnering material lying wholly in the interface plane. The ability to fine tune the transition from Dyakonov surface waves to SPP waves by temperature control may be potentially exploited for temperature-sensing applications and in sub-freezing situations [17], [18].

The plan of this paper is as follows. Section 2 provides the details of the canonical boundary-value problem for surface-wave propagation when the chosen partnering materials occupy the adjacent half-spaces $z < 0$ and $z > 0$. Although the canonical boundary-value problem is practically unimplementable, it lies at the heart of practically implementable configurations such as the prism-coupled, grating-coupled, and waveguide-coupled configurations [1]. Illustrative numerical results are presented in Section 3, and the main conclusions from those results are provided in Section 4. An $\exp(-i\omega t)$ dependence on time t is implicit, with $i = \sqrt{-1}$ and angular frequency ω. Vectors are underlined once, dyadics twice. Column vectors and matrices are enclosed within square brackets. The Cartesian unit vectors are denoted by $\underline{\hat{u}}_x$, $\underline{\hat{u}}_y$, and $\underline{\hat{u}}_z$; the position vector $\underline{r} = x\underline{\hat{u}}_x + y\underline{\hat{u}}_y + z\underline{\hat{u}}_z$; the permittivity and permeability of free space are denoted by ε_0 and μ_0, respectively; $k_0 = \omega\sqrt{\varepsilon_0\mu_0}$ is the free-space wavenumber; $c_0 = 1/\sqrt{\varepsilon_0\mu_0}$ is the speed of light in free space; and the square root operator, denoted by $\sqrt{\cdot}$, delivers the principal square root whose real part is always non-negative.

2. Canonical boundary-value problem

Let us now simplify a general formalism [19] to establish the canonical boundary-value problem for surface-wave propagation guided by the planar interface of a uniaxial material and an isotropic material. The uniaxial material, labeled $\mathcal{A}$, fills the half-space $z > 0$ and is characterized by the relative permittivity dyadic

$$\underline{\underline{\varepsilon}}_{\mathcal{A}} = \varepsilon_{\mathcal{A}}^{\mathrm{s}}\underline{\underline{I}} + \left(\varepsilon_{\mathcal{A}}^{\mathrm{t}} - \varepsilon_{\mathcal{A}}^{\mathrm{s}}\right)\underline{\hat{u}}\,\underline{\hat{u}}, \tag{1}$$

where $\underline{\underline{I}} = \underline{\hat{u}}_x\underline{\hat{u}}_x + \underline{\hat{u}}_y\underline{\hat{u}}_y + \underline{\hat{u}}_z\underline{\hat{u}}_z$ is the identity dyadic [16]. The unit vector $\underline{\hat{u}}$ points in the direction of the optic axis of material $\mathcal{A}$. We have chosen for it to lie in the xy plane, oriented at angle ψ with respect to the x axis, i.e.,

$$\underline{\hat{u}} = \cos\psi\,\underline{\hat{u}}_x + \sin\psi\,\underline{\hat{u}}_y. \tag{2}$$

The dyadic $\underline{\underline{\varepsilon}}_{\mathcal{A}}$ has two eigenvalues: $\varepsilon_{\mathcal{A}}^{\mathrm{s}}$ of algebraic multiplicity [20] equal to 2 and $\varepsilon_{\mathcal{A}}^{\mathrm{t}}$ of algebraic multiplicity equal to 1. Whereas $\varepsilon_{\mathcal{A}}^{\mathrm{s}}$ governs the propagation of *ordinary* plane waves, both eigenvalues together govern the propagation of *extraordinary* plane waves, in material $\mathcal{A}$ [16]. The isotropic material, labeled $\mathcal{B}$, fills the half-space $z < 0$ and is characterized by the relative permittivity dyadic $\varepsilon_{\mathcal{B}}\underline{\underline{I}}$. Both materials are non-magnetic and non-magnetoelectric [21], [22].

The electromagnetic field phasors in the two partnering materials are represented by

$$\left.\begin{aligned}\underline{E}_\ell(\underline{r}) &= \underline{\mathcal{E}}_\ell\,\exp\left(i\underline{k}_\ell \bullet \underline{r}\right)\\ \underline{H}_\ell(\underline{r}) &= \underline{\mathcal{H}}_\ell\,\exp\left(i\underline{k}_\ell \bullet \underline{r}\right)\end{aligned}\right\}, \qquad \ell \in \{\mathcal{A}, \mathcal{B}\}\ . \tag{3}$$

The amplitude vectors $\underline{\mathcal{E}}_\ell$ and $\underline{\mathcal{H}}_\ell$ have complex-valued components, as does the wave vector $\underline{k}_\ell$. All three vectors can vary with ω. Without loss of generality, we consider the surface wave to propagate parallel to $\underline{\hat{u}}_x$ in the xy plane, i.e., $\underline{\hat{u}}_y \bullet \underline{k}_\ell \equiv 0$.

2.1 Half-space $z > 0$

In the half-space $z > 0$, the Maxwell curl postulates yield

$$\left.\begin{aligned} \underline{k}_{\mathcal{A}} \times \underline{\mathcal{E}}_{\mathcal{A}} &= \omega\mu_0 \underline{\mathcal{H}}_{\mathcal{A}} \\ \underline{k}_{\mathcal{A}} \times \underline{\mathcal{H}}_{\mathcal{A}} &= -\omega\varepsilon_0 \underline{\underline{\varepsilon}}_{\mathcal{A}} \bullet \underline{\mathcal{E}}_{\mathcal{A}} \end{aligned}\right\}, \tag{4}$$

where

$$\underline{k}_{\mathcal{A}} = k_0 \left(q\, \hat{\underline{u}}_x + i\alpha_{\mathcal{A}} \hat{\underline{u}}_z \right) \tag{5}$$

and $\text{Re}\,\{\alpha_{\mathcal{A}}\} > 0$ for surface-wave propagation.

On combining (4) and (5), a biquadratic dispersion relation emerges for $\alpha_{\mathcal{A}}$, the four roots being

$$\pm\sqrt{q^2 - \varepsilon^s_{\mathcal{A}}}, \qquad \pm\sqrt{\varepsilon^t_{\mathcal{A}} \left[q^2 \left(\frac{\cos^2\psi}{\varepsilon^s_{\mathcal{A}}} + \frac{\sin^2\psi}{\varepsilon^t_{\mathcal{A}}} \right) - 1 \right]}. \tag{6}$$

The two roots with non-negative real parts are identified as

$$\left.\begin{aligned} \alpha_{\mathcal{A}1} &= \sqrt{q^2 - \varepsilon^s_{\mathcal{A}}} \\ \alpha_{\mathcal{A}2} &= \sqrt{\varepsilon^t_{\mathcal{A}} \left[q^2 \left(\frac{\cos^2\psi}{\varepsilon^s_{\mathcal{A}}} + \frac{\sin^2\psi}{\varepsilon^t_{\mathcal{A}}} \right) - 1 \right]} \end{aligned}\right\}. \tag{7}$$

Accordingly,

$$\left.\begin{aligned} \underline{\mathcal{E}}_{\mathcal{A}} &= A_{\mathcal{A}1}\, \underline{\mathcal{E}}_{\mathcal{A}1} + A_{\mathcal{A}2}\, \underline{\mathcal{E}}_{\mathcal{A}2} \\ \underline{\mathcal{H}}_{\mathcal{A}} &= \sqrt{\frac{\varepsilon_0}{\mu_0}} \left(A_{\mathcal{A}1}\, \underline{\mathcal{H}}_{\mathcal{A}1} + A_{\mathcal{A}2}\, \underline{\mathcal{H}}_{\mathcal{A}2} \right) \end{aligned}\right\}, \tag{8}$$

where

$$\left.\begin{aligned} \underline{\mathcal{E}}_{\mathcal{A}1} &= -i\alpha_{\mathcal{A}1} \sin\psi\, \hat{\underline{u}}_x + i\alpha_{\mathcal{A}1} \cos\psi\, \hat{\underline{u}}_y + q \sin\psi\, \hat{\underline{u}}_z \\ \underline{\mathcal{E}}_{\mathcal{A}2} &= \alpha^2_{\mathcal{A}1} \cos\psi\, \hat{\underline{u}}_x - \varepsilon^s_{\mathcal{A}} \sin\psi\, \hat{\underline{u}}_y + iq\alpha_{\mathcal{A}2} \cos\psi\, \hat{\underline{u}}_z \\ \underline{\mathcal{H}}_{\mathcal{A}1} &= \alpha^2_{\mathcal{A}1} \cos\psi\, \hat{\underline{u}}_x - \varepsilon^s_{\mathcal{A}} \sin\psi\, \hat{\underline{u}}_y + i\alpha_{\mathcal{A}1} q \cos\psi\, \hat{\underline{u}}_z \\ \underline{\mathcal{H}}_{\mathcal{A}2} &= i\alpha_{\mathcal{A}2}\varepsilon^s_{\mathcal{A}} \sin\psi\, \hat{\underline{u}}_x - i\alpha_{\mathcal{A}2}\varepsilon^s_{\mathcal{A}} \cos\psi\, \hat{\underline{u}}_y - \varepsilon^s_{\mathcal{A}} q \sin\psi\, \hat{\underline{u}}_z \end{aligned}\right\}. \tag{9}$$

The scalars q, $A_{\mathcal{A}1}$, and $A_{\mathcal{A}2}$ have to be determined by enforcing boundary conditions across the interface $z = 0$.

2.2 Half-space $z < 0$

In the half-space $z < 0$, the Maxwell curl postulates yield

$$\left.\begin{aligned} \underline{k}_{\mathcal{B}} \times \underline{\mathcal{E}}_{\mathcal{B}} &= \omega\mu_0 \underline{\mathcal{H}}_{\mathcal{B}} \\ \underline{k}_{\mathcal{B}} \times \underline{\mathcal{H}}_{\mathcal{B}} &= -\omega\varepsilon_0\varepsilon_{\mathcal{B}} \underline{\mathcal{E}}_{\mathcal{B}} \end{aligned}\right\} \tag{10}$$

with

$$\underline{k}_{\mathcal{B}} = k_0 \left(q\, \hat{\underline{u}}_x - i\alpha_{\mathcal{B}} \hat{\underline{u}}_z \right), \tag{11}$$

where

$$\alpha_{\mathcal{B}} = \sqrt{q^2 - \varepsilon_{\mathcal{B}}} \tag{12}$$

must be chosen so that Re $\{\alpha_{\mathcal{B}}\} > 0$. Accordingly

$$\left.\begin{aligned} \underline{\mathcal{E}}_{\mathcal{B}} &= A_{\mathcal{B}1}\,\hat{\underline{u}}_y + A_{\mathcal{B}2}\,\left(i\alpha_{\mathcal{B}}\hat{\underline{u}}_x + q\hat{\underline{u}}_z\right) \\ \underline{\mathcal{H}}_{\mathcal{B}} &= \sqrt{\frac{\varepsilon_0}{\mu_0}}\left[A_{\mathcal{B}1}\,\left(i\alpha_{\mathcal{B}}\hat{\underline{u}}_x + q\hat{\underline{u}}_z\right) - A_{\mathcal{B}2}\,\varepsilon_{\mathcal{B}}\hat{\underline{u}}_y\right] \end{aligned}\right\}, \tag{13}$$

with the scalars $A_{\mathcal{B}1}$ and $A_{\mathcal{B}2}$ to be determined by enforcing boundary conditions across the interface $z = 0$.

2.3 Interface z = 0

The continuity of tangential components of the electric and magnetic field phasors across the $z = 0$ imposes the conditions

$$\left.\begin{aligned} -i\alpha_{\mathcal{A}1}\sin\psi A_{\mathcal{A}1} + \alpha_{\mathcal{A}1}^2\cos\psi\, A_{\mathcal{A}2} &= i\alpha_{\mathcal{B}}A_{\mathcal{B}2} \\ i\alpha_{\mathcal{A}1}\cos\psi A_{\mathcal{A}1} - \varepsilon_{\mathcal{A}}^s\sin\psi A_{\mathcal{A}2} &= A_{\mathcal{B}1} \\ \alpha_{\mathcal{A}1}^2\cos\psi A_{\mathcal{A}1} + i\alpha_{\mathcal{A}2}\varepsilon_{\mathcal{A}}^s\sin\psi A_{\mathcal{A}2} &= i\alpha_{\mathcal{B}1}A_{\mathcal{B}1} \\ -\varepsilon_{\mathcal{A}}^s\sin\psi A_{\mathcal{A}1} - i\alpha_{\mathcal{A}2}\varepsilon_{\mathcal{A}}^s\cos\psi A_{\mathcal{A}2} &= -\varepsilon_{\mathcal{B}}A_{\mathcal{B}2} \end{aligned}\right\}. \tag{14}$$

2.4 Dispersion relation

The four conditions (14) may be represented compactly as

$$[M]\cdot\begin{bmatrix} A_{\mathcal{A}1} \\ A_{\mathcal{A}2} \\ A_{\mathcal{B}1} \\ A_{\mathcal{B}2} \end{bmatrix} = \begin{bmatrix} 0 \\ 0 \\ 0 \\ 0 \end{bmatrix} \tag{15}$$

wherein the 4×4 matrix $[M]$ must be singular for surface-wave propagation. The dispersion equation $\det[M] = 0$ is equivalent to the equation

$$\begin{aligned} &\varepsilon_{\mathcal{A}}^s\left(\varepsilon_{\mathcal{B}}\sqrt{q^2-\varepsilon_{\mathcal{A}}^s} + \varepsilon_{\mathcal{A}}^s\sqrt{q^2-\varepsilon_{\mathcal{B}}}\right)\left[\sqrt{q^2-\varepsilon_{\mathcal{B}}} + \sqrt{q^2\left(\frac{\varepsilon_{\mathcal{A}}^t\cos^2\psi}{\varepsilon_{\mathcal{A}}^s} + \sin^2\psi\right) - \varepsilon_{\mathcal{A}}^t}\right]\tan^2\psi \\ &= \sqrt{q^2-\varepsilon_{\mathcal{A}}^s}\left(\sqrt{q^2-\varepsilon_{\mathcal{B}}} + \sqrt{q^2-\varepsilon_{\mathcal{A}}^s}\right) \\ &\quad\times\left[\varepsilon_{\mathcal{B}}\left(q^2-\varepsilon_{\mathcal{A}}^s\right) + \varepsilon_{\mathcal{A}}^s\sqrt{q^2-\varepsilon_{\mathcal{B}}}\sqrt{q^2\left(\frac{\varepsilon_{\mathcal{A}}^t\cos^2\psi}{\varepsilon_{\mathcal{A}}^s} + \sin^2\psi\right) - \varepsilon_{\mathcal{A}}^t}\right]. \end{aligned} \tag{16}$$

The symmetry of (16) is such that if a surface wave exists for angle $\psi = \psi^\star$, then surface waves also exist for $\psi = -\psi^\star$ and $\psi = \pi \pm \psi^\star$.

3. Numerical studies

In order to concentrate on the effects of temperature on the propagation of surface waves guided by the interface of the chosen isotropic and uniaxial materials, we fixed the frequency as 0.6 THz for all numerical results presented here.

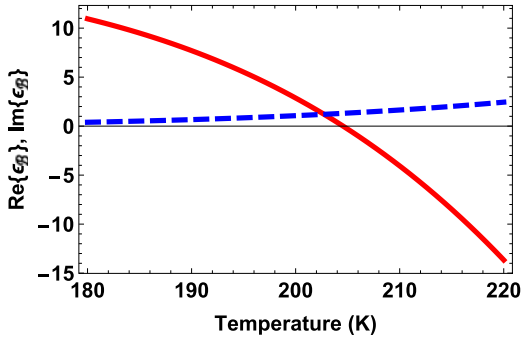

Fig. 1. Re $\{\varepsilon_{\mathcal{B}}\}$ (red solid curve) and Im $\{\varepsilon_{\mathcal{B}}\}$ (blue dashed curve) plotted against $T \in (180, 220)$ K, at a frequency of 0.6 THz.

3.1 Selection of partnering materials

The angular existence domain (i.e., the range of values of ψ) for Dyakonov surface waves is larger for materials which exhibit larger degrees of anisotropy [1], [8]. Accordingly, with the aim of making the effects of temperature more conspicuous, we choose material $\mathcal{A}$ to be highly anisotropic. This may be achieved by taking material $\mathcal{A}$ to be an engineered composite material, arising from the homogenization of two component materials labeled $\mathcal{A}1$ and $\mathcal{A}2$. Both are isotropic dielectric materials, with relative permittivities $\varepsilon_{\mathcal{A}1}$ and $\varepsilon_{\mathcal{A}2}$, and volume fractions $f_{\mathcal{A}1}$ and $f_{\mathcal{A}2} = 1 - f_{\mathcal{A}1}$, respectively. High degrees of anisotropy may be conceptualized on assuming that the component materials are randomly distributed as acicular particles oriented parallel to $\underline{\hat{u}}$. Then, according to the Bruggeman homogenization formalism [22], the relative permittivity parameters of material $\mathcal{A}$ are estimated to be [23]

$$\left.\begin{aligned} \varepsilon_{\mathcal{A}}^{\mathrm{s}} &= \frac{1}{2}\left[\left(f_{\mathcal{A}2} - f_{\mathcal{A}1}\right)\left(\varepsilon_{\mathcal{A}2} - \varepsilon_{\mathcal{A}1}\right) + \sqrt{\left[\left(f_{\mathcal{A}2} - f_{\mathcal{A}1}\right)\left(\varepsilon_{\mathcal{A}2} - \varepsilon_{\mathcal{A}1}\right)\right]^2 + 4\varepsilon_{\mathcal{A}1}\varepsilon_{\mathcal{A}2}} \right] \\ \varepsilon_{\mathcal{A}}^{\mathrm{t}} &= f_{\mathcal{A}1}\varepsilon_{\mathcal{A}1} + f_{\mathcal{A}2}\varepsilon_{\mathcal{A}2} \end{aligned}\right\} . \tag{17}$$

Alternatively, a laminated composite material could be employed for the sought-after high degree of anisotropy [22].

For component material $\mathcal{A}1$ we chose free space, i.e., $\varepsilon_{\mathcal{A}1} = 1.0$, while for component material $\mathcal{A}2$ we chose zirconium–tin–titanate whose relative permittivity at 0.6 THz has the approximately constant value of $\varepsilon_{\mathcal{A}2} = 37.20 + 0.40i$ from 180 K to 220 K [24]. The volume fraction of free space was fixed at $f_{\mathcal{A}1} = 0.58$. Thus, (17) yield $\varepsilon_{\mathcal{A}}^{\mathrm{s}} = 3.96 + 0.01i$ and $\varepsilon_{\mathcal{A}}^{\mathrm{t}} = 16.38 + 0.17i$.

Material $\mathcal{B}$ was taken to be the semiconductor InSb, whose relative permittivity in the terahertz regime is given by the Drude model [25], [26]

$$\varepsilon_{\mathcal{B}} = \varepsilon_{\infty} - \frac{\omega_p^2}{\omega^2 + i\gamma\omega} \tag{18}$$

wherein the high-frequency relative permittivity $\varepsilon_{\infty} = 15.68$, the damping constant $\gamma = \pi \times 10^{11}$ rad s^{-1}, and the plasma frequency $\omega_p = \sqrt{N q_e^2 / 0.015\,\varepsilon_0\, m_e}$ depends upon the electronic charge $q_e = -1.60 \times 10^{-19}$ C and mass $m_e = 9.11 \times 10^{-31}$ kg. The dependance of $\varepsilon_{\mathcal{B}}$ on temperature T (in K) is mediated by the intrinsic carrier density (in m^{-3}) [27]–[29]

$$N = 5.76 \times 10^{20}\, T^{3/2} \exp\left(-\frac{E_{\mathrm{g}}}{2k_B T}\right) \tag{19}$$

with $E_{\mathrm{g}} = 0.26$ eV being the bandgap and $k_B = 8.62 \times 10^{-5}$ eV K^{-1} being the Boltzmann constant.

The real and imaginary parts of $\varepsilon_{\mathcal{B}}$ are plotted against temperature $T \in (180, 220)$ K at 0.6 THz frequency in Fig 1. Whereas $\varepsilon_{\mathcal{B}} = 10.95 + 0.39i$ at $T = 180$ K , $\varepsilon_{\mathcal{B}} = -13.66 + 2.44i$ at $T = 220$ K. Thus, material $\mathcal{B}$ is a dissipative dielectric material at $T = 180$ K but a metal at $T = 220$ K, with Re $\{\varepsilon_{\mathcal{B}}\} = 0$ at $T \approx 204.56$ K.

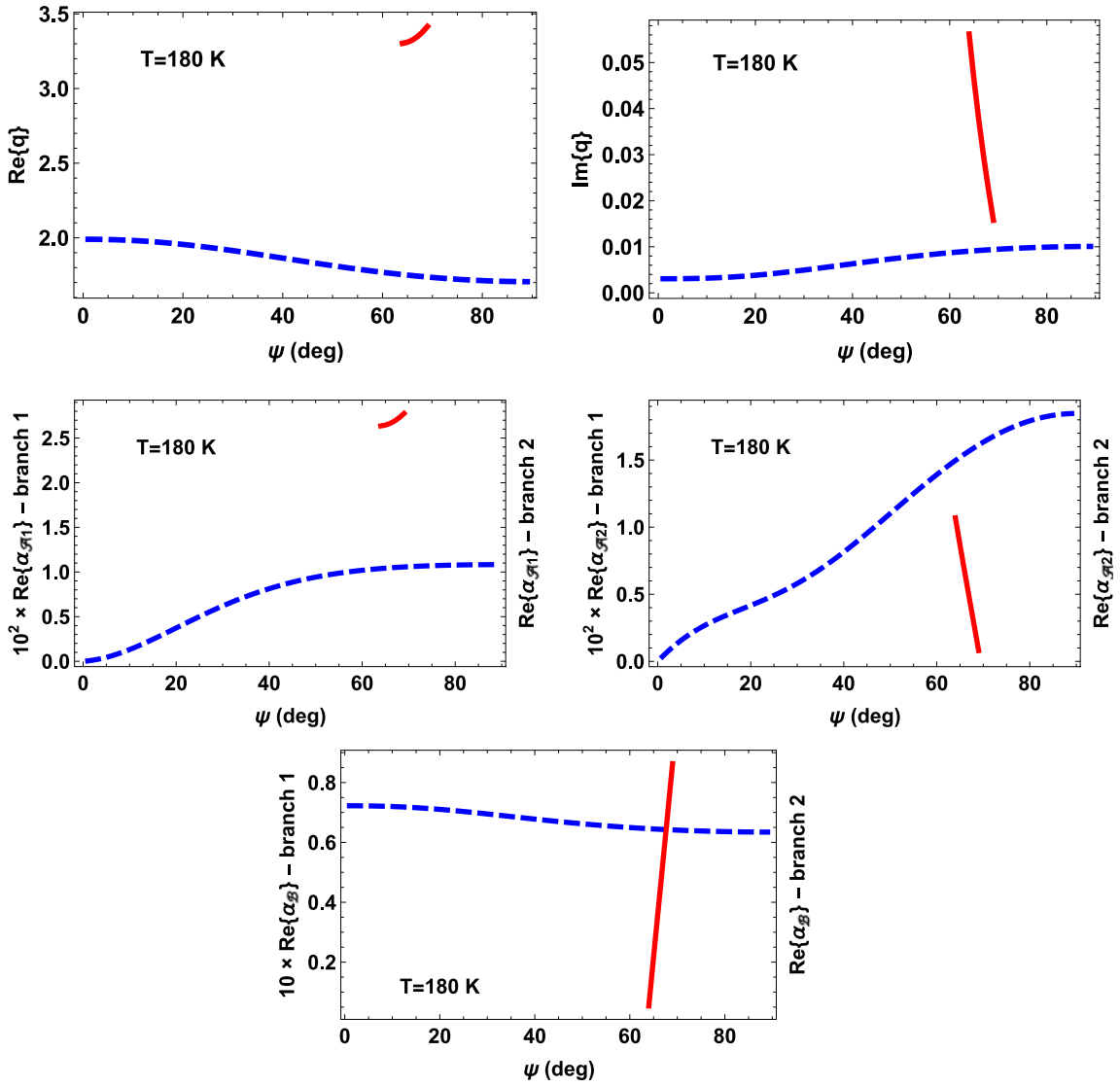

Fig. 2. Re $\{q\}$, Im $\{q\}$, Re $\{\alpha_{\mathcal{A}1}\}$, Re $\{\alpha_{\mathcal{A}2}\}$, and Re $\{\alpha_{\mathcal{B}}\}$ plotted against $\psi \in [0^\circ, 90^\circ]$ for $T = 180$ K (i.e., $\varepsilon_{\mathcal{B}} = 10.95 + 0.39i$). Solution branch 1 (blue dashed curves) exists for $\psi \in (0^\circ, 90^\circ)$, and solution branch 2 (red solid curves) exists for $\psi \in (64^\circ, 69^\circ)$.

3.2 Surface-wave analysis

Let us now delineate the effect on surface-wave propagation of increasing the temperature from the dissipative-dielectric regime to the metallic regime for material $\mathcal{B}$ by means of numerical studies.

3.2.1 $T = 180$ K: We begin at $T = 180$ K, material $\mathcal{B}$ being a weakly dissipative dielectric material at that temperature. The real and imaginary parts of the normalized propagation constant q, as extracted from (16), are plotted against the orientation angle ψ in Fig. 2. Also plotted in Fig. 2 are the real parts of the decay constants $\alpha_{\mathcal{A}1}$ and $\alpha_{\mathcal{A}2}$, as delivered by (7), and $\alpha_{\mathcal{B}}$, as delivered by (12).

The surface-wave solutions found can be organized into two branches: branch 1 which exists for $\psi \in (0^\circ, 90^\circ)$ and branch 2 which exists for $\psi \in (64^\circ, 69^\circ)$. Thus, two distinct Dyakonov surface waves can propagate for $\psi \in (64^\circ, 69^\circ)$.

Solutions on branch 2 have considerably higher values of Re $\{q\}$ than solutions on branch 1. Therefore, values of the phase speed $v_{ph} = c_0/\text{Re}\,\{q\}$ on branch 2 are considerably lower than

on branch 1. In addition, since Im $\{q\}$ has generally much larger values on branch 2 than on branch 1, surface waves on branch 2 generally decay much more rapidly along $\underline{\hat{u}}_x$ than those on branch 1. The real parts of $\alpha_{\mathcal{A}1}$ and $\alpha_{\mathcal{A}2}$ are two orders of magnitude larger on branch 2 than on branch 1, and the real part of $\alpha_{\mathcal{B}}$ is an order of magnitude larger on branch 2 than on branch 1. Therefore, surface waves on branch 2 are much more tightly bound to the interface $z = 0$ than surface waves on branch 1, especially so in the half-space $z > 0$.

The surface waves at $T = 180$ K must be classified as Dyakonov surface waves, because they require both partnering materials to be homogeneous and at least one partnering material to be anisotropic. Since the original works on Dyakonov surface waves [4], [5] dealt with the planar interface of nondissipative materials, it is of interest to compare the results presented in Fig. 2 with results for the scenarios wherein one or both of the partnering materials are nondissipative. In Fig. 3, the variations of q against $\psi \in [0^\circ, 90^\circ]$ are presented for the same parameter values used for Fig. 2 but for the following three cases:

a) Im $\left\{\varepsilon_{\mathcal{A}}^s\right\} = 0$ and Im $\left\{\varepsilon_{\mathcal{A}}^t\right\} = 0$, but Im $\{\varepsilon_{\mathcal{B}}\} \neq 0$;
b) Im $\left\{\varepsilon_{\mathcal{A}}^s\right\} \neq 0$ and Im $\left\{\varepsilon_{\mathcal{A}}^t\right\} \neq 0$, but Im $\{\varepsilon_{\mathcal{B}}\} = 0$;
c) Im $\left\{\varepsilon_{\mathcal{A}}^s\right\} =$ Im $\left\{\varepsilon_{\mathcal{A}}^t\right\} =$ Im $\{\varepsilon_{\mathcal{B}}\} = 0$.

For case a), the solutions can be organized into two branches: branch 1, which exists for $\psi \in (49^\circ, 90^\circ)$, and branch 2, which exists for $\psi \in (64^\circ, 69^\circ)$. Thus, two distinct Dyakonov surface waves are possible for $\psi \in (64^\circ, 69^\circ)$ and one for $\psi \in (49^\circ, 64^\circ) \cup (69^\circ, 90^\circ)$ but none at all for $\psi \in (0^\circ, 49^\circ)$. For case (b), the solutions can be organized into three branches: branch 1 which exists for $\psi \in (0^\circ, 59^\circ)$, branch 2 which exists for $\psi \in (64^\circ, 69^\circ)$, and branch 3 which exists for $\psi \in (71^\circ, 90^\circ)$. Thus, there is at most one solution for $\psi \in [0^\circ, 90^\circ]$, and no solution for $\psi \in (59^\circ, 64^\circ) \cup (69^\circ, 71^\circ)$. For case (c), there is only one solution branch as expected [5], [8], and our numerical results show that it exists for $\psi \in (64^\circ, 69^\circ)$. Indeed, a more precise value for the angular existence domain for case (c), namely $(63.73^\circ, 69.43^\circ)$, is provided by an analytical formula [5].

By comparing Figs. 2 and 3, we infer that the multiple solution branches that arise for Fig. 2 are due to the nonzero imaginary parts of $\varepsilon_{\mathcal{A}}^{s,t}$ and/or $\varepsilon_{\mathcal{B}}$. Parenthetically, the very large angular existence domains that arise for cases (a) and (b) in Fig. 3 are attributable to the highly anisotropic nature of material $\mathcal{A}$. Even for case (c), the angular existence domain is about 5° for the same reason; with natural materials, the angular existence domain is about 1° and smaller [7], [8].

3.2.2 $T = 190$ K: Now, let us increase the temperature to $T = 190$ K. At this temperature, $\varepsilon_{\mathcal{B}} = 7.70 + 0.66i$. The plots of Re $\{q\}$, Im $\{q\}$, Re $\{\alpha_{\mathcal{A}1}\}$, Re $\{\alpha_{\mathcal{A}2}\}$, and Re $\{\alpha_{\mathcal{B}}\}$ versus ψ are provided in Fig. 4. The surface-wave solutions found can be organized into four branches: branch 1 exists for $\psi \in (38^\circ, 68^\circ)$, branch 2 for $\psi \in (48^\circ, 59^\circ)$, branch 3 for $\psi \in (56^\circ, 90^\circ)$, and branch 4 for $\psi \in (0^\circ, 7^\circ)$. Either none, one, two, or three distinct Dyakonov surface waves can exist for $\psi \in (0^\circ, 90^\circ)$.

Dyakonov surface waves on branch 2 have quite distinct characteristics from those on branches 1, 3, and 4. Specifically, the surface waves on branch 2 have lower phase speeds, decay more rapidly along the propagation direction, and are much more tightly bound to the interface $z = 0$ (especially in the halfspace $z > 0$) than the surface waves on the other three branches. Again, dissipation in the partnering materials is responsible for the number of solution branches exceeding unity.

3.2.3 $T = 200$ K: Increasing the temperature to $T = 200$ K, at which $\varepsilon_{\mathcal{B}} = 2.87 + 1.07i$, has a dramatic effect on the surface-wave solutions. This may be appreciated from Fig. 5 wherein the plots analogous to those given in Figs. 2 and 4 are presented. Here, there is only one solution branch, and it spans $\psi \in (0^\circ, 90^\circ)$. In other words, a Dyakonov surface wave exists for every $\psi \in (0^\circ, 90^\circ)$, the angular existence domain being the maximum possible due to the partnering materials being dissipative.

As compared to the surface waves on branches labeled 2 for $T = 180$ K and 190 K, the surface waves at $T = 200$ K have a rather larger phase speed, decay more slowly along $\underline{\hat{u}}_x$, and are slightly less tightly bound to the interface $z = 0$.

3.2.4 $T = 205$ K: Further increasing the temperature so that the real part of $\varepsilon_{\mathcal{B}}$ changes from being small in magnitude and positive valued to being small in magnitude and negative valued

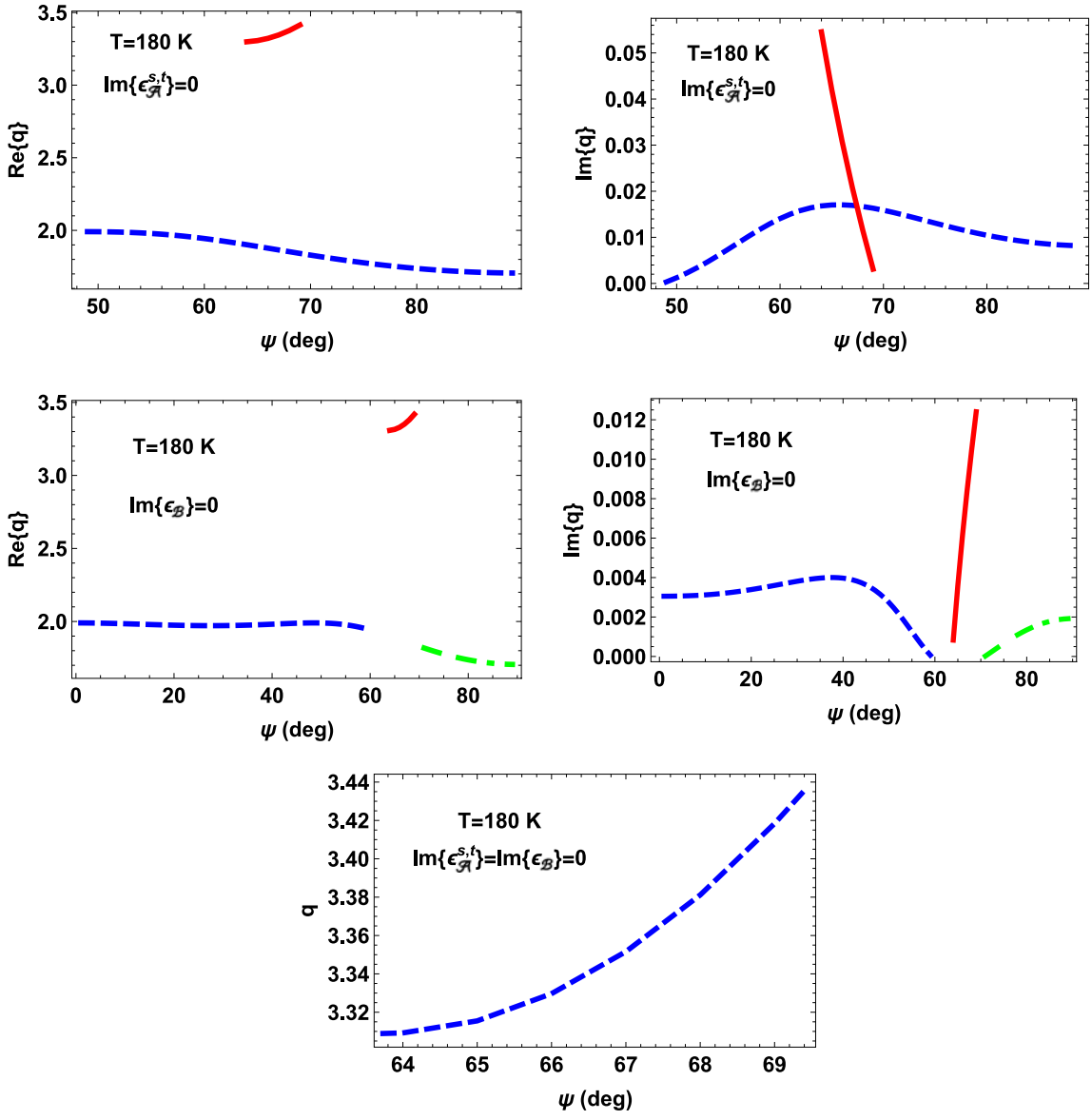

Fig. 3. As in Fig. 2, Re $\{q\}$ and Im $\{q\}$ plotted against ψ for $T = 180$ K but for (top row) Im $\{\varepsilon_{\mathcal{A}}^{s}\} = 0$ and Im $\{\varepsilon_{\mathcal{A}}^{t}\} = 0$, but Im $\{\varepsilon_{\mathcal{B}}\} \neq 0$; (middle row) Im $\{\varepsilon_{\mathcal{A}}^{s}\} \neq 0$ and Im $\{\varepsilon_{\mathcal{A}}^{t}\} \neq 0$, but Im $\{\varepsilon_{\mathcal{B}}\} = 0$; and (bottom row) Im $\{\varepsilon_{\mathcal{A}}^{s}\} =$ Im $\{\varepsilon_{\mathcal{A}}^{t}\} =$ Im $\{\varepsilon_{\mathcal{B}}\} = 0 \Rightarrow$ Im $\{q\} = 0$. Top row: solution branch 1 (blue dashed curves) exists for $\psi \in (49^\circ, 90^\circ)$ and solution branch 2 (red solid curves) exists for $\psi \in (64^\circ, 69^\circ)$. Middle row: solution branch 1 (blue dashed curves) exists for $\psi \in (0^\circ, 59^\circ)$, solution branch 2 (red solid curves) exists for $\psi \in (64^\circ, 69^\circ)$, and solution branch 3 (green broken dashed curves) exists for $\psi \in (71^\circ, 90^\circ)$. Bottom row: the sole solution branch exists for $\psi \in (63.73^\circ, 69.43^\circ)$, as yielded by an analytical formula [5] and confirmed by numerical studies here.

makes only a relatively modest difference to the surface-wave solutions, as may be appreciated from Fig. 6. This figure contains the plots analogous to those given in Figs. 2, 4, and 5 but for $T = 205$ K (i.e., $\varepsilon_{\mathcal{B}} = -0.30 + 1.33i$). As for $T = 200$ K, at $T = 205$ K there is only one surface-wave solution and it exists for all $\psi \in (0^\circ, 90^\circ)$. The surface waves at $T = 205$ K must be classified as SPP waves because Re $\{\varepsilon_{\mathcal{B}}\} < 0$.

As compared with the Dyakonov surface waves at $T = 200$ K, the SPP waves at $T = 205$ K have rather larger phase speeds, decay more quickly along the propagation direction in the xy plane, and are slightly more tightly bound to the interface $z = 0$ in the half-space $z < 0$.

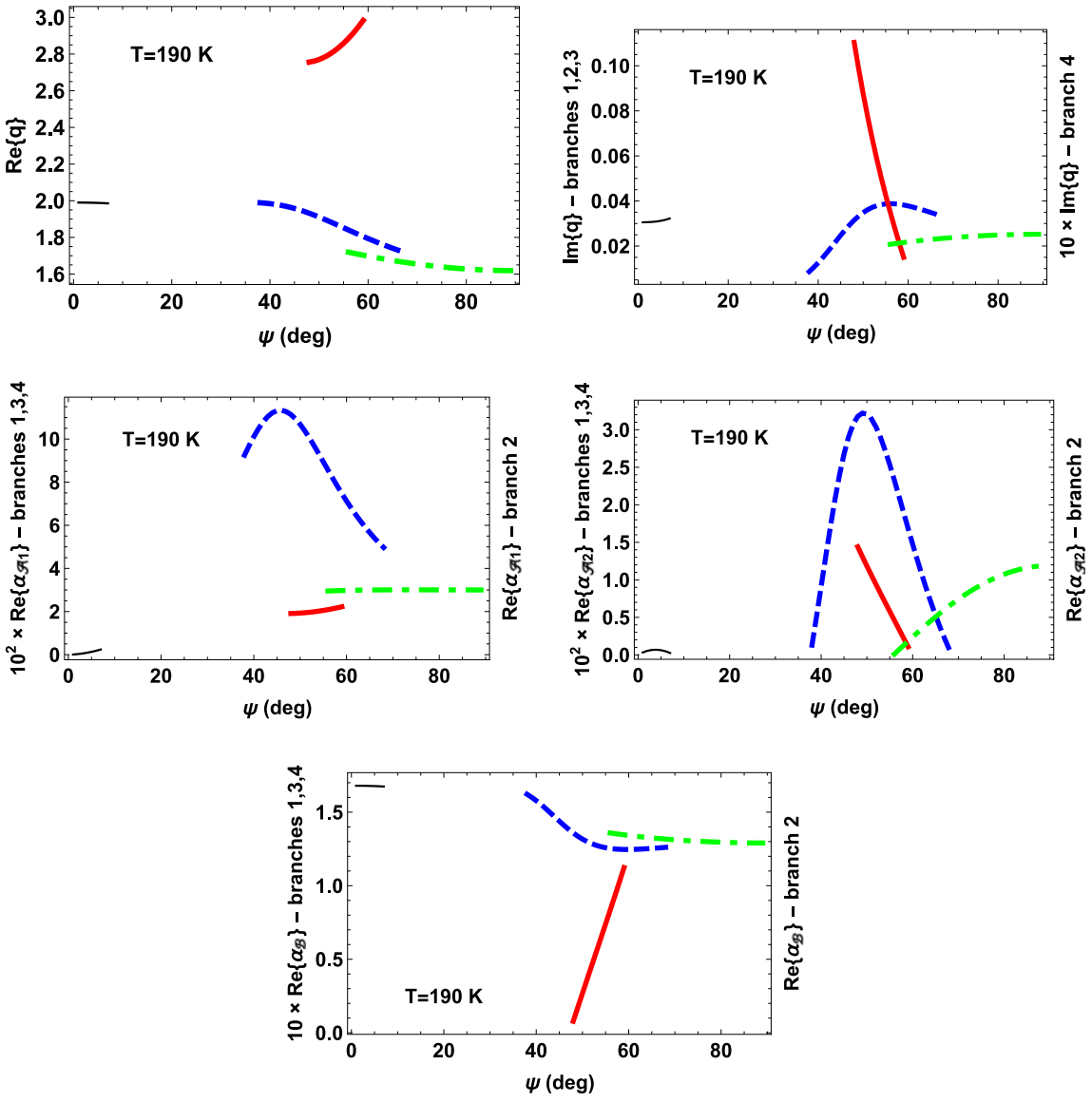

Fig. 4. As Fig. 2 except that $T = 190$ K (i.e., $\varepsilon_{\mathcal{B}} = 7.70 + 0.66i$). Solution branch 1 (blue dashed curves) exists for $\psi \in (38^\circ, 68^\circ)$, solution branch 2 (red solid curves) exists for $\psi \in (48^\circ, 59^\circ)$, solution branch 3 (green dashed-dotted curves) exists for $\psi \in (56^\circ, 90^\circ)$, and solution branch 4 (black thin solid curves) exists for $\psi \in (0^\circ, 7^\circ)$.

3.2.5 $T = 220$ K: Finally, let us increase the temperature to $T = 220$ K so that $\varepsilon_{\mathcal{B}} = -13.66 + 2.44i$. As revealed in Fig. 7, there are two branches of surface-wave solutions: branch 1 exists for $\psi \in (0^\circ, 67^\circ)$ and branch 2 for $\psi \in (76^\circ, 90^\circ)$. There are no solutions for $\psi \in (67^\circ, 76^\circ)$. Thus, at most one SPP wave can propagate for $\psi \in (0^\circ, 90^\circ)$.

In comparison to the SPP waves on branch 2, those on branch 1 have lower phase speeds, decay more quickly along the propagation direction and are substantially more tightly bound to the interface $z = 0$ (especially in the half-space $z > 0$).

The absence of solutions for $\psi \in (67^\circ, 76^\circ)$ in Fig. 7 merits further discussion. While SPP-wave propagation guided by the planar interface of an isotropic dielectric material and an isotropic metal is possible for all ψ, the incorporation of a uniaxial dielectric material to partner the metal can dramatically change this [30]–[32]. Unlike the simple SPP-wave-propagation scenario wherein

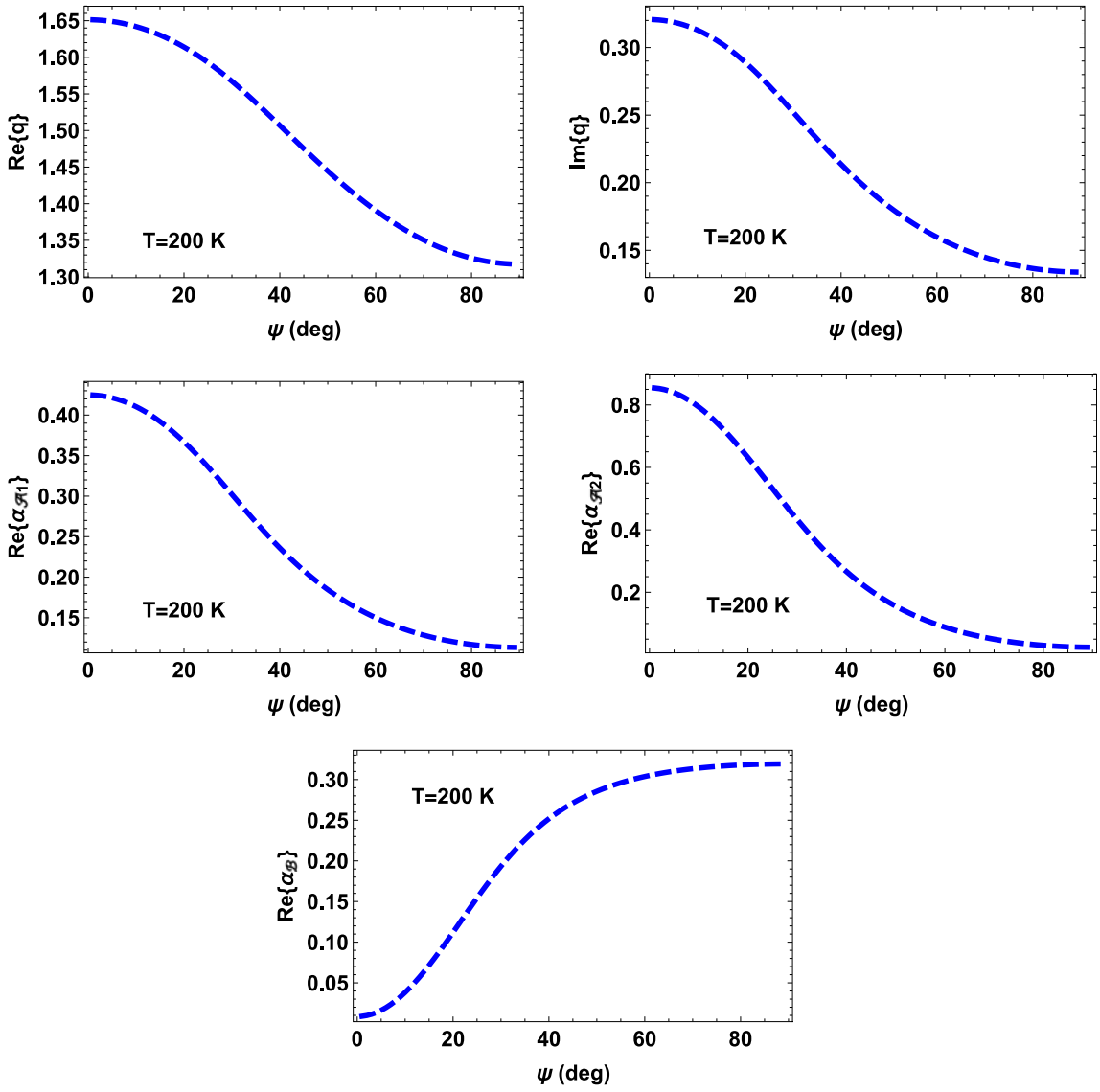

Fig. 5. As Fig. 2, except that $T = 200$ K (i.e., $\varepsilon_{\mathcal{B}} = 2.87 + 1.07i$). The sole solution branch exists for $\psi \in (0^\circ, 90^\circ)$.

both partnering materials are isotropic [2], [3], when the partnering dielectric material is uniaxial, the SPP wave on the metal side of the planar interface is generally composed of both *s*- and *p*-polarized components. As a result, either *s*- or *p*-polarized incident light can excite the SPP wave, in general [1]. Similarly, the SPP wave on the dielectric side of the planar interface comprises both ordinary and extraordinary components, whose relative magnitudes and phases depend upon the direction of propagation. One (and only one) solution of the dispersion equation exists for all ψ when $\varsigma \equiv \varepsilon_{\mathcal{A}}^{\mathrm{t}}/\varepsilon_{\mathcal{A}}^{\mathrm{s}} = 1$ [2], [3]; the same can be expected when ς does not deviate too much from unity [30], but SPP-wave propagation may not be possible for all ψ when ς is substantially different from unity, as is evident from Fig. 7 for $\varsigma = 4.136 + 0.032i$.

4. Discussion and closing remarks

We investigated the changes that occur with temperature in the character of surface-wave propagation guided by the planar interface of a temperature-sensitive isotropic material and a

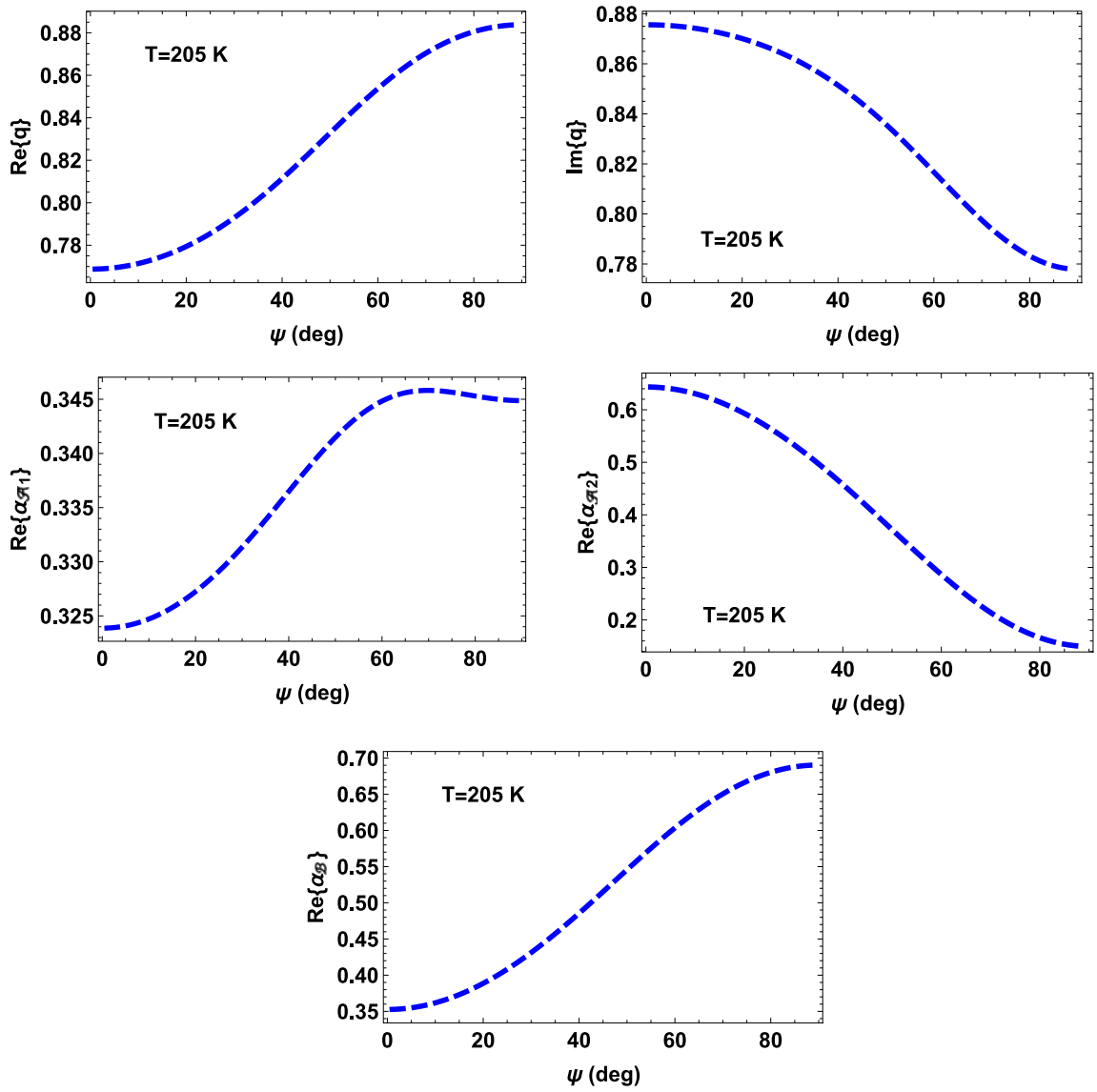

Fig. 6. As Fig. 2, except that $T = 205$ K (i.e., $\varepsilon_{\mathcal{B}} = -0.30 + 1.33i$). The sole solution branch exists for $\psi \in (0^\circ, 90^\circ)$.

temperature-insensitive uniaxial material, each characterized by a relative permittivity dyadic and the optic axis of the uniaxial partnering material lying wholly in the interface plane. Over the temperature range considered, the real part of the relative permittivity scalar of the isotropic partnering material changes from positive to negative and, thus, that material changes from being a weakly dissipative dielectric material to a metal.

At the lower temperatures, at which the isotropic material behaves as a weakly dissipative material, only one surface wave that is tightly bound to the planar interface propagates, and the angular existence domain for this surface wave is relatively small; other surface waves that are not tightly bound to the planar interface also propagate, and the angular existence domains for these surface waves are much larger. All of these waves are Dyakonov surface waves. Multiple Dyakonov surface waves may propagate in a specific direction.

At higher temperatures, at which the isotropic material behaves as a weakly dissipative metal, only one SPP wave propagates for a substantial (and even complete) range of ψ from 0° to 90°,

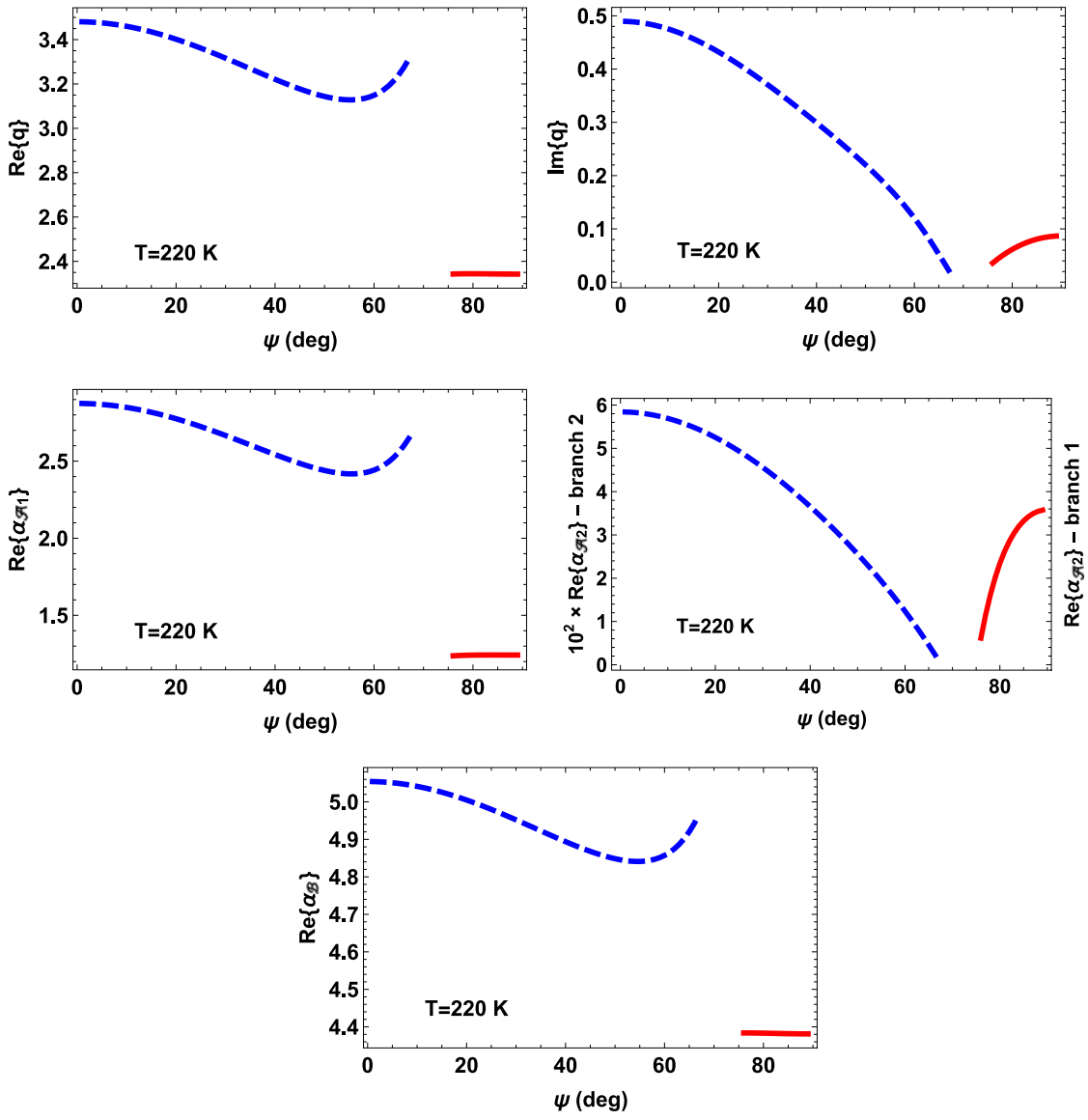

Fig. 7. As Fig. 2, except that $T = 220$ K (i.e., $\varepsilon_{\mathcal{B}} = -13.66 + 2.44i$). Solution branch 1 (blue dashed curves) exists for $\psi \in (0^\circ, 67^\circ)$ and solution branch 2 (red solid curves) exists for $\psi \in (76^\circ, 90^\circ)$.

tightly bound to the interface $z = 0$. There may be a range of ψ for which surface-wave propagation does not occur.

At intermediate temperatures, at which the real part of the relative permittivity of the isotropic material is close to zero, only one surface wave propagates. This surface wave does so in all directions and it is tightly bound to the interface $z = 0$. It can be classified either as a Dyakonov surface wave or as a SPP wave, depending on the sign of Re $\{\varepsilon_{\mathcal{B}}\}$.

The preceding numerical study clearly demonstrates that the character of surface waves can be highly sensitive to temperature. For the particular example investigated, the numbers of propagating surface waves, their angular existence domains, their propagation constants, and their decay constants, could all be dramatically altered by varying the temperature, over the regimes that allow the propagation of Dyakonov surface waves and surface-plasmon-polariton waves. The ability to thermally tune surface-wave characteristics may be potentially exploited for low-temperature applications in the terahertz regime [33].

References

[1] J. A. Polo, Jr., T. G. Mackay, and A. Lakhtakia, *Electromagnetic Surface Waves: A Modern Perspective*. Waltham, MA, USA: Elsevier, 2013.
[2] J. M. Pitarke, V. M. Silkin, E. V. Chulkov, and P. M. Echenique, "Theory of surface plasmon and surface-plasmon polaritons," *Rep. Prog. Phys.*, vol. 70, no. 1, pp. 1–87, 2007.
[3] S. A. Maier, *Plasmonics: Fundamentals and Applications*. New York, NY, USA: Springer, 2007.
[4] F. N. Marchevskiĭ, V. L. Strizhevskiĭ, and S. V. Strizhevskiĭ, "Singular electromagnetic waves in bounded anisotropic media," *Sov. Phys. Solid State*, vol. 26, no. 5, pp. 911–912, 1984.
[5] M. I. D'yakonov, "New type of electromagnetic wave propagating at an interface," *Sov. Phys. JETP*, vol. 67, no. 4, pp. 714–716, 1988.
[6] D. B. Walker, E. N. Glytsis, and T. K. Gaylord, "Surface mode at isotropic-uniaxial and isotropic-biaxial interfaces," *J. Opt. Soc. Amer. A*, vol. 15, no. 1, pp. 248–260, 1998.
[7] O. Takayama, L. Crasovan, D. Artigas, and L. Torner, "Observation of Dyakonov surface waves," *Phys. Rev. Lett.*, vol. 102, no. 4, Jan. 2009, Art. no. 043903.
[8] O. Takayama, L.-C. Crasovan, S. K. Johansen, D. Mihalache, D. Artigas, and L. Torner, "Dyakonov surface waves: A review," *Electromagnetics*, vol. 28, no. 3, pp. 126–145, Mar. 2008.
[9] M. Shinn and W. M. Robertson, "Surface plasmon-like sensor based on surface electromagnetic waves in a photonic band-gap material," *Sens. Actuators B: Chem.*, vol. 105, no. 2, pp. 360–364, Mar. 2005.
[10] V. N. Konopsky and E. V. Alieva, "Photonic crystal surface waves for optical biosensors," *Anal. Chem.*, vol. 79, no. 12, pp. 4729–4735, May 2007.
[11] I. Abdulhalim, M. Zourob, and A. Lakhtakia, "Surface plasmon resonance for biosensing: A mini-review," *Electromagnetics*, vol. 28, no. 3, pp. 214–242, Mar. 2008.
[12] J. S. Sekhon and S. S. Verma, "Plasmonics: The future wave of communication," *Curr. Sci. India*, vol. 101, no. 4, pp. 484–488, Aug. 2011.
[13] O. Takayama, D. Artigas, and L. Torner, "Practical dyakonons," *Opt. Lett.*, vol. 37, no. 20, pp. 4311–4313, 2012.
[14] V. E. Ferry, L. A. Sweatlock, D. Pacifici, and H. A. Atwater, "Plasmonic nanostructure design for efficient light coupling into solar cells," *Nano Lett.*, vol. 8, no. 12, pp. 4391–4397, Nov. 2008.
[15] L. Liu *et al.*, "Planar light concentration in micro-Si solar cells enabled by a metallic grating–photonic crystal architecture," *ACS Photonics*, vol. 3, no. 4, pp. 604–610, Mar. 2016.
[16] H. C. Chen, *Theory of Electromagnetic Waves*. New York, NY, USA: McGraw–Hill, 1983.
[17] H. H. Sample and L. G. Rubin, "Instrumentation and methods for low temperature measurements in high magnetic fields," *Cryogen.*, vol. 17, no. 11, pp. 597–606, Nov. 1977.
[18] J. W. Ekin, *Experimental Techniques for Low-Temperature Measurements: Cryostat Design, Material Properties and Superconductor Critical-Current Testing*. Oxford, U.K.: Oxford Univ. Press, 2006.
[19] J. A. Polo, Jr., S. R. Nelatury, and A. Lakhtakia, "Propagation of surface waves at the planar interface of a columnar thin film and an isotropic substrate," *J. Nanophoton.*, vol. 1, no. 1, Jan. 2007, Art. no. 013501.
[20] H. Lütkepohl, *Handbook of Matrices*. Chicester, U.K.: Wiley, 1996.
[21] T. H. O'Dell, *The Electrodynamics of Magneto–Electric Media*. Amsterdam, The Netherlands: North-Holland, 1970.
[22] T. G. Mackay and A. Lakhtakia, *Modern Analytical Electromagnetic Homogenization*. San Rafael, CA, USA: Morgan & Claypool, 2015.
[23] T. G. Mackay, "Towards metamaterials with giant dielectric anisotropy via homogenization: An analytical study," *Photon. Nanostruct.—Fundam. Appl.*, vol. 13, no. 1, pp. 8–19, Jan. 2015.
[24] K. Berdel, J. G. Rivas, P. Bolívar, P. de Maagt, and H. Kurz, "Temperature dependence of the permittivity and loss tangent of high-permittivity materials at terahertz frequencies," *IEEE Trans. Microw. Theory Tech.*, vol. 53, no. 4, pp. 1266–1271, Apr. 2005.
[25] S. C. Howells and L. A. Schlie, "Transient terahertz reflection spectroscopy of undoped InSb from 0.1 to 1.1 THz," *Appl. Phys. Lett.*, vol. 69, no. 4, pp. 550–552, Jul. 1996.
[26] J. Han and A. Lakhtakia, "Semiconductor split-ring resonators for thermally tunable terahertz metamaterials," *J. Modern Opt.*, vol. 56, no. 4, pp. 554–557, Feb. 2009.
[27] R. W. Cunningham and J. B. Gruber, "Intrinsic concentration and heavy-hole mass in InSb," *J. Appl. Phys.*, vol. 41, no. 4, pp. 1804–1809, Mar. 1970.
[28] M. Oszwaldowski and M. Zimpel, "Temperature dependence of intrinsic carrier concentration and density of states effective mass of heavy holes in InSb," *J. Phys. Chem. Solids*, vol. 49, no. 10, pp. 1179–1185, 1988.
[29] P. Halevi and F. Ramos-Mendieta, "Tunable photonic crystals with semiconducting constituents," *Phys. Rev. Lett.*, vol. 85, no. 9, pp. 1875–1878, Aug. 2000.
[30] S. J. Elston and J. R. Sambles, "Surface plasmon-polaritons on an anisotropic substrate," *J. Modern Opt.*, vol. 37, no. 12, pp. 1895–1902, 1990.
[31] R. A. Depine and M. L. Gigli, "Resonant excitation of surface modes at a single flat uniaxial-metal interface," *J. Opt. Soc. Amer. A*, vol. 14, no. 2, pp. 510–519, Feb. 1997.
[32] I. Abdulhalim, "Surface plasmon TE and TM waves at the anisotropic film-metal interface," *J. Opt. A: Pure Appl. Opt.*, vol. 11, no. 1, Jan. 2009, Art. no. 015002.
[33] H.-J. Song and T. Nagatsuma, *Handbook of Terahertz Technologies: Devices and Applications*. Boca Raton, FL, USA: CRC, 2015.